Earth and Planetary Science Letters 362 (2013) 258–271

Contents lists available at SciVerse ScienceDirect

Earth and Planetary Science Letters

journal homepage: www.elsevier.com/locate/epsl

Mantle dynamics and characteristics of the Azores plateau

C. Adam [a,*], P. Madureira [a,b], J.M. Miranda [c], N. Lourenço [c,d], M. Yoshida [e], D. Fitzenz [a,1]

[a] Centro de Geofísica de Évora/Univ. Évora, 7002-554 Évora, Portugal
[b] Estrutura de Missão para a Extensão da Plataforma Continental (EMEPC), 2770-047, Paço d' Arcos, Portugal
[c] Instituto Portugues do Mar e da Atmosfera, Lisboa, Portugal
[d] University of Algarve, IDL, Campus de Gambelas, 8000 Faro, Portugal
[e] Institute for Research on Earth Evolution (IFREE), Japan Agency for Marine-Earth Science and Technology (JAMSTEC), Yokosuka, Kanagawa 237-0061, Japan

ARTICLE INFO

Article history:
Received 25 July 2012
Received in revised form
2 November 2012
Accepted 5 November 2012
Editor: T. Spohn
Available online 18 January 2013

Keywords:
Azores triple junction
mantle dynamics
dynamic topography
lithospheric stresses
tectonic regimes

ABSTRACT

Situated in the middle of the Atlantic Ocean, the Azores plateau is a region of elevated topography encompassing the triple junction between the Eurasian, Nubian and North American plates. The plateau is crossed by the Mid-Atlantic Ridge, and the Terceira Rift is generally thought of as its northern boundary. The origin of the plateau and of the Terceira Rift is still under debate. This region is associated with active volcanism. Geophysical data describe complex tectonic and seismic patterns. The mantle under this region is characterized by anomalously slow seismic velocities. However, this mantle structure has not yet been used to quantitatively assess the influence of the mantle dynamics on the surface tectonics. In this study, we use a highly resolved tomography model to model the convection occurring in the mantle beneath the Azores region. The convection pattern points out two distinct upwelling, thus proving that the volcanism emplacement is created by a buoyant mantle upwelling. The modeled dynamic topography recovers well the characteristics of the depth anomaly associated with the Azores plateau, except for the south-eastern most part, thus proving that most of the depth anomaly associated with the Azores plateau is created by the present-day mantle dynamics. The stresses induced by the mantle convection can account for the rifting regime observed over the Azores plateau and the Terceira Rift, and its consequences in terms of surface morphology and seismicity.

1. Introduction

The Azores plateau, a region of elevated topography (Fig. 1), encompasses the boundary zone where three major tectonic plates Eurasia, Nubia and North America meet to form the Azores Triple Junction. The plateau is asymmetric relative to the Mid-Atlantic Ridge (MAR). The eastern side of the plateau, the zone our study focuses on, has an approximate triangular shape. It is delimited by two major tectonic discontinuities: the Mid-Atlantic Ridge (MAR) to the west, and the Terceira Rift (TR) to the north-east. The East Azores fracture Zone constitutes its southern boundary. It contains numerous seamounts and seven of the Azores islands: Faial, Pico, S. Jorge, Graciosa and Terceira for the central group, S. Miguel and S. Maria in the eastern group.

Several hypotheses were proposed for the plateau formation. Some invoke only a tectonic origin. The enhanced upwelling and magmatism would then be driven by plate-boundary forces. Luis et al. (1994) show that there has been a northward jump of the Azores triple junction, during which the Azores region would have been transferred from the Nubian plate to the Eurasian plate. Luis et al. (1994) think that this mechanism is the result of small changes in the relative motion between the three megaplates. They also considered that this mechanism would be responsible for the "disturbed" topography. For Luis and Neves (2006), the elevation of the Azores plateau is mainly due to thickened crust, whereas the presence of buoyant material at the base of the crust is also required to partially account for the uplift of the plateau.

For others, the presence of the Azores plume is necessary to explain the observations. For example, Yang et al. (2006) agree with the jump of the Azores triple junction but argue that the latter is triggered by the relative motion between the lithospheric plate and an underlying mantle plume. Vogt and Jung (2004) also mention the role of the plume in the plateau formation. This later would have been formed by successive NE jumps of the oblique spreading axis, where the present TR is the latest stage. For Gente et al. (2003), the plateau results from the interaction between the MAR and the plume, followed by the progressive southward rifting of the plateau after 7 Ma. According to different authors the beginning of the enhanced volcanism occurred around 10 Ma, and ended between 3 and 7 Ma depending upon latitude (Cannat et al., 1999; Escartín et al., 2001; Gente et al., 2003; Maia et al.,

* Corresponding author.
E-mail address: adam@uevora.pt (C. Adam).
[1] Now at RMS, Inc, Newark, CA, USA.

0012-821X/$ - see front matter © 2012 Elsevier B.V. All rights reserved.
http://dx.doi.org/10.1016/j.epsl.2012.11.014

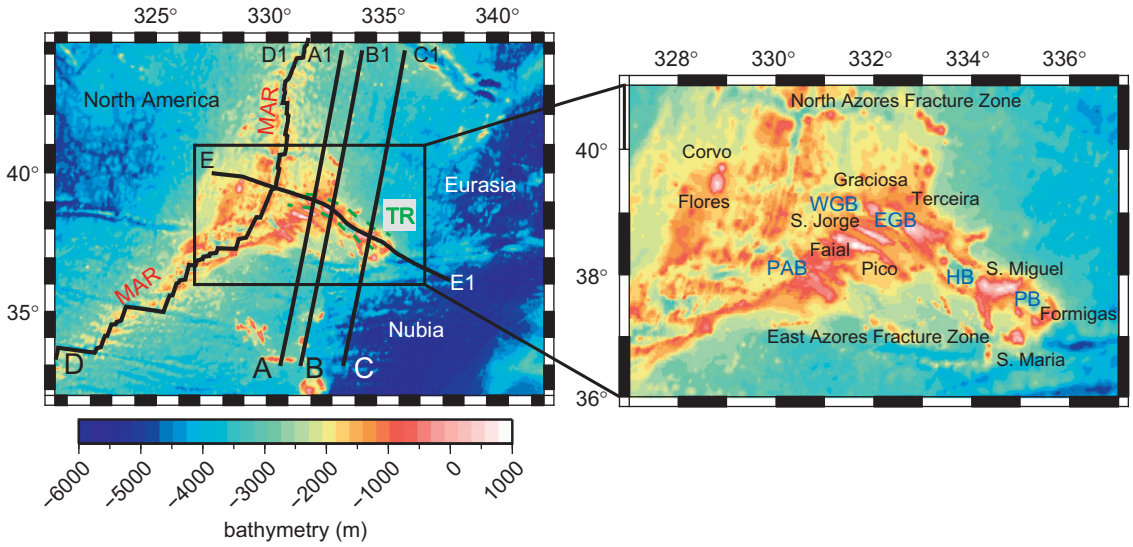

Fig. 1. Bathymetry of the Azores region. (a) global view (b) focus on the Azores islands. The volcanism is still active on most of the islands. MAR: Mid-Atlantic Ridge; TR: Terceira Rift; WGB: Western Graciosa Basin; EGB: Eastern Graciosa Basin; HB: Hirondelle Basin; PB: Povoação Basin; PAB: Princess Alice Bank.

2001). However, active volcanism is still reported near shore and on several of the Azores islands (Machado, 1959; Self, 1976; Moore, 1990; Cole et al., 1995, 2001; Gaspar et al., 2003).

Since the paroxysmal phase of plateau build-up by enhanced volcanism, rifting would have been the major process in controlling the volcanism emplacement and the shaping of the plateau. Indeed, through a careful analysis of the bathymetry, Lourenço et al. (1998) show that the tectonics of the Azores region is controlled by two sets of conjugates faults with strikes N120° and N150°, which would constrain the volcanism emplacement and thus the morphology of the bathymetric features. Two kinds of volcanic features coexist in the study area. Despite the presence of roughly circular to elliptical islands such as Graciosa and Terceira, the predominant features are volcanic ridges elongated along the N120° and N150° directions. Lourenço et al. 1998 hypothesize that such features could be explained if one considers the Azores region as a transfer zone, broadly in a tectonic transtensional regime, which accommodates the motion between the MAR and the dextral Gloria fault.

Several studies have focused on the seismicity pattern in the area. The seismicity is concentrated along the MAR and the TR. The seismic pattern along the TR is quite complex. Previous research (Miranda et al., submitted for publication) reported extension perpendicular to the N120°E associated with graben subsidence and extensive volcanism, particularly west of Terceira Island. Borges et al. (2007) define two zones of distinct seismicity and stress direction, showing the existence of two different domains east and west of Terceira Island, broadly corresponding to the above strikes. None of those studies addressed the physical phenomena constraining this partitioning.

The Terceira Rift is supposed to constitute the northeast boundary of the eastern Azores plateau. It is a succession of deep basins (reaching more than 3000 m deep) and volcanic highs encompassing from the west to the east, the west Graciosa basin, the Graciosa island, the east Graciosa basin, the Terceira island, the north Hirondelle basin, D. João de Castro Bank, south Hirondelle basin, S. Miguel island, the Povoação Basin, and the Formigas islets. The wavelength separating these geological features is 60–100 km. Several hypothesis have been proposed for its interpretation: as a secondary spreading ridge in a RRR configuration developed in the sequence of a major change in plate kinematics (Krause and Watkins, 1970), as the result of oblique extension (McKenzie, 1972), or even as a leaky transform (Madeira and Ribeiro, 1990). Vogt and Jung (2004) interpreted it as one of the results of a specific hyperslow spreading regime. The TR trends WNW–ESE, a direction that also characterizes the main geologic features to the south namely the S. Jorge Island, Faial-Pico ridge and Princess Alice bank (Fig. 1).

The Azores region has been considered a classic example of a hotspot-ridge interaction. Several geophysical (Schilling, 1985; Cannat et al., 1999; Gente et al., 2003; Yang et al., 2006) and geochemical (Morgan, 1971; Schilling, 1985; White et al., 1979; Bougault and Treuil, 1980; Bougault and Cande, 1985; Dosso et al., 1999; Moreira et al., 1999; Madureira et al., 2005, 2011) studies point out the influence of a mantle plume. The plume is imaged by several tomography models (Silveira and Stutzmann, 2002; Silveira et al., 2006; Montelli et al., 2004; Yang et al., 2006). The characteristics of the plume do nevertheless vary according to the models, namely in what concerns the wavelength and amplitude of the velocity anomalies, as well as the depth of the root: is the 'Azores plume' a shallow feature of the upper mantle or does it extend to the whole mantle? However, such models of the mantle structure have not yet been used to quantitatively assess the influence of the mantle on the surface observations. The importance of this evaluation is also strengthened by the absence of correlation between the plate boundary geometry and the patterns of magmatism or the crust thickness observed over the Azores domain (Georgen and Sankar, 2010). That will be our goal in the present study. We will use the P-wave velocity model designed by Yang et al. (2006). It is derived from teleseismic body waves recorded by six broadband seismic stations on the Azores Islands and its fine resolution is able to resolve the narrow mantle plume. We will convert the seismic velocity anomalies into density anomalies and model the convection driven by these density anomalies. The approach used to model the mantle convection and the resulting stresses will be described in Section 2. We will compare the convection pattern with the volcanism emplacement in order to assess a possible link between them. We will then compare the dynamic topography to the depth anomaly characterized through a method especially adapted to the bathymetry filtering. The stresses imposed at the base of the lithosphere by the underlying mantle convection will be compared with the morphology of the seafloor and the islands, and with the seismicity pattern. We will also use the stress tensor computed from our convection model to predict the tectonic regimes. Finally, we will discuss the pertinence of our local study, and the new insights our results bring on the understanding of the dynamics and tectonics of the Azores region.

2. Model

2.1. Mantle structure

2.1.1. Conversion of seismic velocity anomalies into density anomalies

Our study uses as an input the velocity anomalies provided by tomography models. Deriving quantitative geodynamical interpretation from tomography models is a difficult task. In order to obtain insightful geodynamic information from tomography models, one needs to convert the velocity anomalies provided by these models into temperature or density anomalies. It is an important step if one aims for example to obtain an accurate characterization of lateral viscosity variations in the mantle, or if one wants to retrieve quantitative information from the tomography models. For a realistic employment of tomography models, we have been striving to integrate the results of mineral physics (Karato, 2008) in our models. These studies describe the depth dependency of the coefficient of thermal expansivity α, and of the temperature derivative of the seismic velocities anomalies for S waves as well as for P waves ($A_{VT} \equiv \partial \ln V / \partial T$). In this study, we will use the α and A_{VT} given by the text book of Karato (2008). The dependency of the density to velocity heterogeneity ratio $R_{\rho/v}$ on these parameters can be obtained through:

$$R_{\rho/V} = \frac{\alpha}{A_{VT}} \tag{1}$$

The density anomaly ($\delta\rho$) can then be obtained through

$$\frac{\delta\rho}{\rho_{ref}} = R_{\rho/V} \frac{\delta v}{v_{ref}} \tag{2}$$

where δv is the seismic velocities anomaly and ρ_{ref} and v_{ref} the reference density and velocity provided in our study by the PREM model (Dziewonski and Anderson, 1981) when the S40RTS model (Ritsema et al., 2011) is used, and by the IASP91 (Kennett and Engdahl, 1991) model when Yang et al. (2006) model is used.

2.1.2. Viscosity model

Viscosity models are generally depth and temperature dependent. The depth dependency often imposes a highly viscous lithosphere between depths 0 and 100 km. However, in the present study, imposing a 100 km high viscosity lithosphere may not be the most appropriate approach. Indeed, our study area encompasses two spreading centers (the MAR and the TR). Imposing a high viscosity lithosphere, would mask these structures and may lead to the omission of the most important dynamics of the study area. Therefore our models will include a lithosphere which thickens away from the MAR as described by the half-space model. To obtain the theoretical lithospheric thickness given by the half-space model, we compute a new seafloor age grid obtained by of the magnetic isochrones interpreted by Luis and Miranda (2008) for the Eurasia–North America plate pair, and by Luis et al. (2009) for the Nubia–Eurasia plate pair. In this case, we will use the density anomaly derived from the tomography model and add a

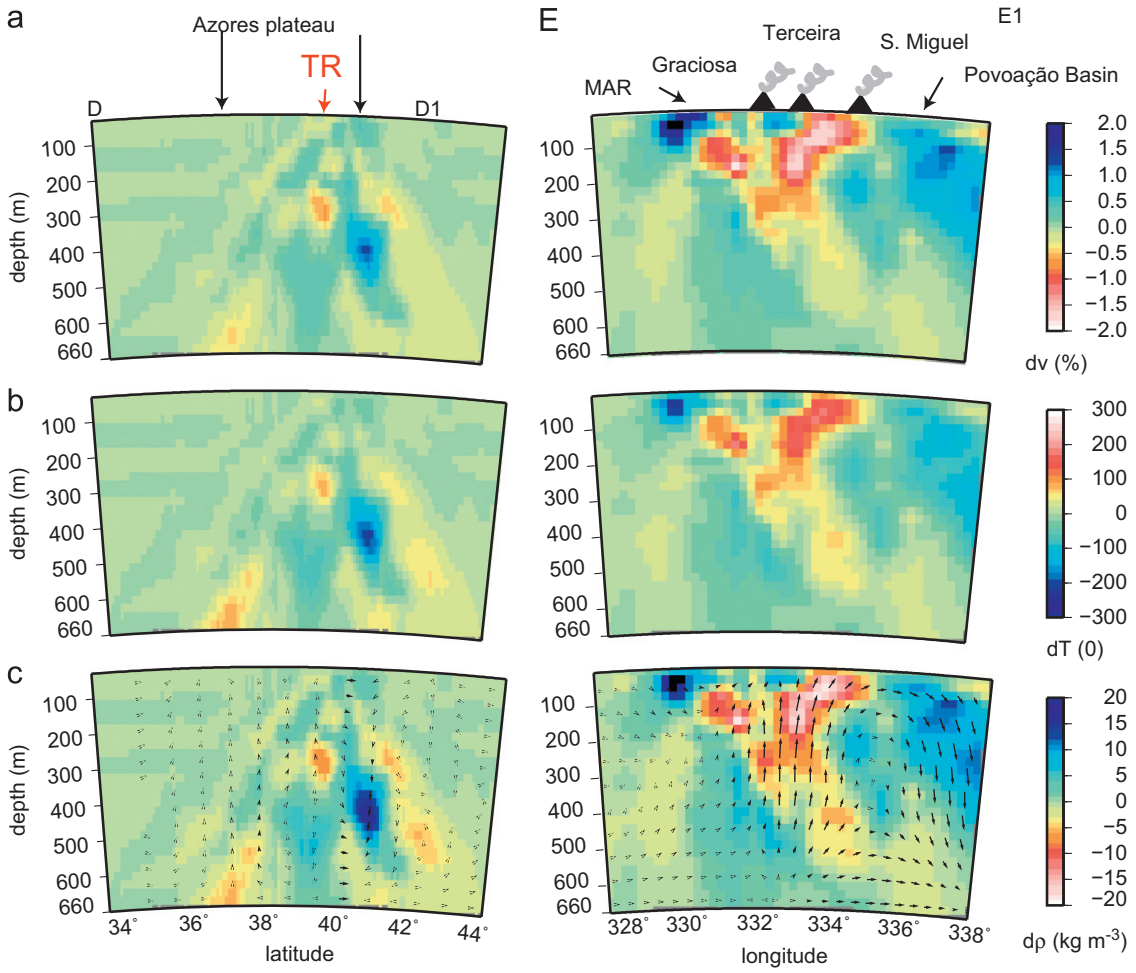

Fig. 2. Depth cross sections along the MAR (left panels) and the TR (right panels); (a) tomography model (Yang et al., 2006); (b) temperature anomalies deduced from the tomography model; (c) density anomalies deduced from the tomography model; the arrows represent the convection driven by these density anomalies.

30 kg m^{-3} anomaly at the theoretical emplacement of the lithosphere. We will also tests the classically employed 100 km thick lithosphere and discuss the influence of the lithosphere characteristics.

We consider the effect of the temperature-dependent viscosity on the mantle convection using an Arrhenius-type viscosity form:

$$\eta = \eta(d)\exp\left(\frac{H_a}{R(T_{ref}+\delta T)} - \frac{H_a}{RT_{ref}}\right) \quad (3)$$

where H_a is the activation enthalpy of mantle rock, R is the gas constant (8.31 kJ mol^{-1}), T_{ref} is the reference temperature, and $\delta T = T - T_{ref}$ is the temperature anomaly. It can be computed from the density anomaly through the equation of state, $\delta\rho = -\alpha_{ref}\rho_{ref}\delta T$. We used the typical values of the upper mantle for the density, ρ_{ref}=3500 kg m^{-3}, the thermal expansivity, $\alpha_{ref}=2.5\times10^{-5}$ K^{-1}, and temperature, T=1500 K. Since the upper mantle is dominated by diffusion creep in dry olivine, we consider the value of the activation enthalpy of the olivine, ($H_a\sim$740 kJ mol^{-1}, Turcotte and Schubert, 2001).

Illustrations of the mantle structure in our study area are provided in Figs. 2 and 3. In Fig. 2, the upper panel shows the velocity anomaly provided by Yang et al. (2006) tomography model. In the middle and lower panels we show the temperature and density anomalies obtained through the computation previously described.

The viscosity laws we employ are illustrated in Fig. 4. The black profile shows the mean value of the viscosity in our study area when a highly viscous lithosphere is imposed between depths 0 and 100 km. The red profile represents a viscosity profile near the MAR (latitude 37.8°N and longitude 328°E) when the depth dependency includes a lithosphere which thickens away from the MAR as described by the half space model. The viscosity obtained with the latter law under the S. Miguel island (latitude 37.8°N and longitude 334.6°E) is illustrated by the blue profile. We can see that in this case, the lithosphere in the vicinity of the MAR (red profile) is much thinner that the one under older seafloor (blue profile).

2.2. Numerical model

After converting the velocity anomalies provided by the tomography models into density anomalies, we model the convection induced by these density anomalies. To model the instantaneous mantle flow induced by the density anomalies, we solve the conservation equations of mass and momentum. In a regional threedimensional spherical shell geometry, along spherical polar coordinates (r, θ, φ), these dimensionless equations are

$$\nabla\cdot v = 0 \quad (4)$$

$$-\nabla p + \nabla\cdot\{\eta(\nabla v + \nabla v^{tr})\} + R_{ai}\delta\rho\, e_r = 0 \quad (5)$$

where v is the velocity vector, p the dynamic pressure, η the viscosity, $\delta\rho$ the density anomaly, R_{ai} the instantaneous Rayleigh number and e_r, the unit vector in the radial direction. The superscript tr indicates the tensor transpose.

The instantaneous Rayleigh number R_{ai} (Yoshida, 2008) used in our computation is given by

$$R_{ai} \equiv \frac{\rho_0 g b^3}{\kappa_0\eta_0} \quad (6)$$

where ρ_0 is the reference density, g the gravitational acceleration, κ_0 the reference thermal diffusivity, η_0 the reference viscosity, and b the mantle thickness considered in the model. The physical values used in this study are listed in Table 1.

The calculation of the instantaneous mantle flow in the regional three-dimensional spherical shell geometry has been performed using the finite-volume (FV) based mantle convection code ConvRS (Yoshida, 2008; Adam et al., 2010). The computation domain extends between latitudes 31.8°N and 44.8°N, and longitudes 320°E and 342.2°E. We consider the convection occurring in the upper mantle, since Yang et al. (2006) tomography model does not describe the whole lower mantle. The number of FVs used is 32

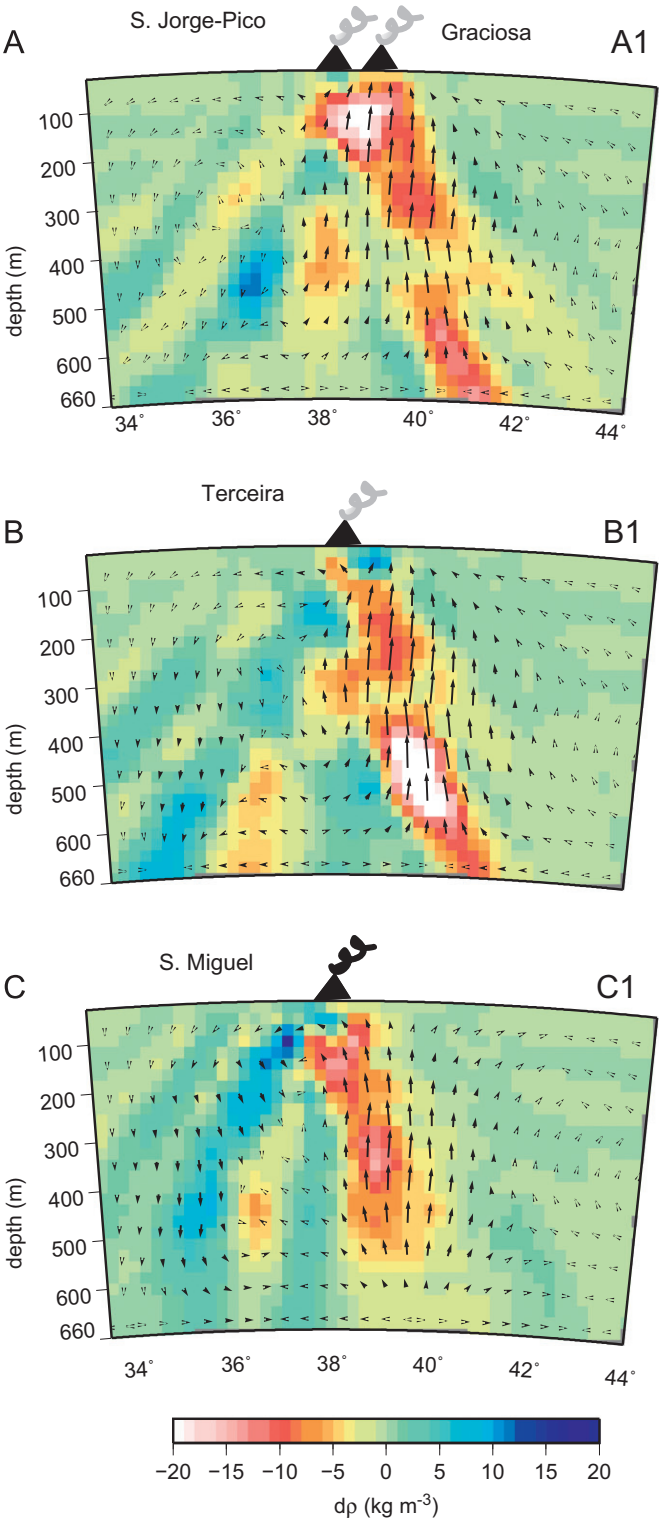

Fig. 3. Depth cross sections along the profiles AA1, BB1. CC1. The color map represent the density anomaly deduced from Yang et al. (2006) tomography model. The arrows represent the convection driven by these density anomalies.

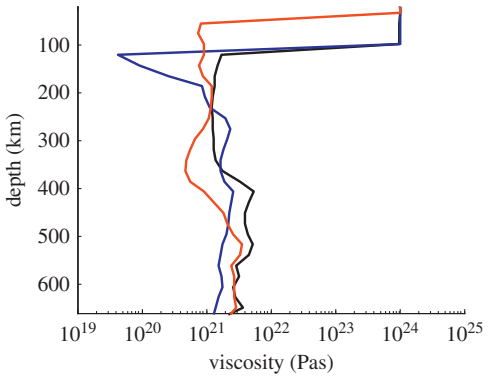

Fig. 4. Viscosity profiles used in our study. The black profile shows the mean value of the viscosity in our study area when a highly viscous lithosphere is imposed between depths 0 and 100 km. The red profile represents a viscosity profile near the MAR (latitude 37.8° N and longitude 328°E) when the depth dependency includes a lithosphere which thickens away from the MAR as described by the half space model. The viscosity obtained with the latter law under the S. Miguel island (latitude 37.8° N and longitude 334.6°E) is illustrated by the blue profile.

Table 1
Physical values used in this study.

Meaning of symbols	Value
Gravitational acceleration at the surface, g	9.81 m s^{-2}
Seawater density, ρ_w	1030 kg m^{-3}
Sediments density, ρ_s	2400 kg m^{-3}
Crust density, ρ_c	2900 kg m^{-3}
Mantle density, ρ_m	3350 kg m^{-3}
Model thickness, b	660 km
Reference density, ρ_0	3350 kg m^{-3}
Reference viscosity in the upper mantle, η_0	10^{21} Pa s
Reference thermal diffusivity, κ_0	10^{-6} m^2 s^{-1}
Instantaneous Rayleigh number, R_{ai}	9.45×10^7
Density contrast between the mantle and sea water, $\Delta\rho_s$	2320 kg m^{-3}
Gravitational constant, G	6.66726×10^{-11} Nm^2/kg^2

(in r) $\times$ 64 (in θ) $\times$ 112 (in φ), which means that the numerical resolutions is 0.2° in the horizontal directions and 22 km in the radial direction. The impermeable and shear stress-free conditions are adopted on the top and bottom surface boundaries. The flows across lateral boundaries are taken to be symmetric

Once we obtain the velocity and the stress field of the instantaneous mantle flow, the dynamic topography can be computed.

The resulting normal stress acting on the top surface boundary (σ_{rr}) is

$$\sigma_{rr} = -p + 2\eta\frac{\partial v_r}{\partial r} \tag{7}$$

where v_r is the radial velocity. The dynamic topography δh is obtained from the normal stress through the equation:

$$\delta h = \frac{\sigma_{rr} - \langle\sigma_{rr}\rangle}{\Delta\rho_s g} \tag{8}$$

where $\langle\sigma_{rr}\rangle$ is the averaged σ_{rr} over the top surface boundary, $\Delta\rho_s$ the density contrast between the mantle and sea water and g, the gravity acceleration.

At the base of the lithosphere, we are considering the viscous shear stress $\tau_{r\theta}$ $\tau_{r\varphi}$.

$$\tau_{r\theta} = \eta\left(\frac{1}{r}\frac{\partial v_r}{\partial\theta} + \frac{\partial v_\theta}{\partial r} - \frac{v_\theta}{r}\right) \tag{9}$$

$$\tau_{r\varphi} = \eta\left(\frac{1}{r\sin(\theta)}\frac{\partial v_r}{\partial\varphi} + \frac{\partial v_\varphi}{\partial r} - \frac{v_\varphi}{r}\right) \tag{10}$$

where v_θ and v_φ are the velocities along the latitude and longitude respectively.

3. Results

3.1. Convection pattern and mantle characteristics

As stated earlier, we use the tomography model of Yang et al. (2006). Depth cross sections of this tomography model along the MAR and the TR are displayed in Fig. 2. Depth cross sections of the density anomalies derived from the tomography model along profiles perpendicular to the TR are displayed in Fig. 3. The seismic velocity anomaly along the MAR varies between -0.5% and 1%. Along the TR, this variation is more important: $\pm2\%$. This implies temperature variations between 300 and -300 °C, and density anomalies variations between -20 and $+20$ kg m^{-3}.

On the depth cross sections along the TR (Fig. 2), the model points out two main low velocity (low density, in red) anomalies in the shallow mantle (depths <200 km), that converge to the same anomaly at a deeper level. One of the shallow anomalies is centered on the group of islands formed by Faial, Pico, S. Jorge, and Graciosa. The other shallow anomaly is located between the Terceira and S. Miguel islands. They create two separate mantle upwellings towards the Rift segments and surface volcanoes. This can be related with the mantle heterogeneity recognized for the Azores plume. Moreover, this pattern can explain the difference of the geochemical signatures observed in sampled lavas, in particular the unique isotopic ratios (Sr, Nd, Pb, He) found in lavas from S. Miguel Island (White et al., 1979; Davies et al., 1989; Turner et al., 1997; Moreira et al., 1999; Beier et al., 2007; Elliott et al., 2007). We also notice the existence of positive density anomaly regions (cold mantle) represented by blue colors. Interestingly, one of these regions is located beneath the Terceira Island, where the most primitive He and Ne were found within the Azores archipelago (Moreira et al., 1999; Madureira et al., 2005). This can be related to the contribution of a sub-continental lithospheric mantle component to the signature of Terceira lavas as recently shown by Madureira et al. (2011). However, it must be stressed that the isotopic signature of Terceira lavas also argue for a plume component with a signature much closer to that sampled by Graciosa and S. Jorge lavas than that interpreted from S. Miguel lavas. As can be observed from Fig. 2, the colder mantle regions create downwelling flows, thus forming a complex convection pattern that arises from their interaction with the upwelling mantle.

On the depth cross sections along the profiles perpendicular to the TR (Fig. 3), the slow velocity area, or 'plume' is located slightly north of the TR. It seems to encompass the whole upper mantle, and is characterized by negative densities in order of 20 kg m^{-3}. A small discontinuity is noticed around the 400 km depth. The southern side of the TR, i.e. the region beneath the Azores plateau is generally faster (or colder), except for an isolated 'blob' situated between the 300–660 km depth interval. This slower (or warmer) area is located at latitude 38°N on the profiles crossing Graciosa Island. It could be at the origin of the volcanism occurring at Pico and S. Jorge islands. To the east, this anomaly is located deeper in the mantle, and becomes smaller and fainter. The amplitude of the anomaly located south of the TR is much smaller (~5–7 kg m^{-3}) and seems to be connected to the very warm area north of the TR. Despite the previously described warm anomaly beneath the Azores plateau, the mantle is generally cooler under this region. This configuration creates a 600 km wide convection

cell which upwelling initiates north of the TR, and which downwelling occurs around the latitude 35°N. It creates the dynamic topography discussed in the following section.

3.2. Depth anomaly and dynamic topography

The Azores plateau has been described by Lourenço et al. (1998) as an area of shallow seafloor with an overall triangular shape, encompassing about 400,000 km^2, roughly delimited by the 2000 m isobath. To characterize more precisely the depth anomaly associated with the Azores plateau, we first correct the bathymetry grid [we used a local bathymetry grid, mostly made from swath bathymetry data, (Miranda, personal communication)] for sediment loading, through the method described in Adam and Bonneville (2005). We then compute the depth anomaly, which is the difference between the bathymetry, corrected for sediments loading, and a theoretical depth, predicted by models of thermal subsidence of the lithosphere, which describe the evolution of the seafloor depth with its age. We use here the GDH1 thermal model (Stein and Stein, 1992). To obtain the theoretical depth given by the GDH1 model, we computed a new seafloor age grid obtained by interpolation of the magnetic isochrones interpreted by Luis and Miranda (2008) for the Eurasia-North America plate pair, and by Luis et al. (2009) for the Nubia–Eurasia plate pair. Afterwards, we filter the depth anomaly through the MiFil (Minimization+Filtering) method (Adam et al., 2005). This method, especially designed to filter depth anomalies consists in minimizing the depth anomaly grid, with a minimizing filter of radius r, then applying a median filter of radius R to the minimized grid. The width of the islands and seamounts we try to eliminate is of the order of 100–150 km. Therefore, the best filtering parameters for characterizing the depth anomaly associated with the Azores plateau are r =30 km and R=250 km.

The obtained depth anomaly is represented in Fig. 5. This 500 km long 300 km wide depth anomaly is elongated along the TR direction (N120°). This swell encompasses the TR but its maxima is located slightly south, between the S. Jorge Island, west, and S. Miguel Island, east. The amplitude of the depth anomaly is about 2000 m. Along the depth-cross sections displayed in Fig. 6, we can see that the swell's maximum is shifted slightly south from the islands location.

The dynamic topography is represented in Fig. 7. We have displayed the results of three models: one with a constant viscosity (Fig. 7a) and two others where the viscosity is depth and temperature dependent (Fig. 7b and c). The dynamic topography displayed in Fig. 7(b) includes a 100 km thick lithosphere, whereas the dynamic topography displayed in Fig. 7(c) has been computed by imposing the thickening of the lithosphere relatively to the MAR, as described by the half-space model. The dynamic topographies computed with a model in which the viscosity is depth and temperature dependent are roughly similar.

The computed dynamic topography recovers the characteristics of the swell. Indeed, the amplitude of the dynamic topography reaches 2000 m. This 500 km long and 300 km wide feature is also elongated along the TR. Some disparities can however be noticed. The dynamic topography does not recover the swell observed east of S. Miguel. This is due to the fact that the mantle is not particularly hot to the east of S. Miguel Island. On the contrary, the velocity anomalies imaged by the tomography model point out a fast zone between depths 0–100 km, east (Fig. 2) and south (Fig. 3) of S. Miguel. If the origin of this fast zone is thermal, these fast velocities can be interpreted as a cold region, which induces downwelling flows which create the negative dynamic topography. It could be correlated with the Povoção basin. We notice however a small shift (~50 km) between the Povoção basin and the negative dynamic topography east of S. Miguel. This could be due to a miscalculation in the derivation of the tomography model, or to the fact that the lithosphere is modeled here as a highly viscous layer, when is should be considered as a visco-plastic or a visco-elasto-plastic layer. The observed positive depth anomaly, east of S. Miguel, as well as the southernmost part of the swell, situated between latitude 37°–38°N and longitudes 333°–334°E, likely

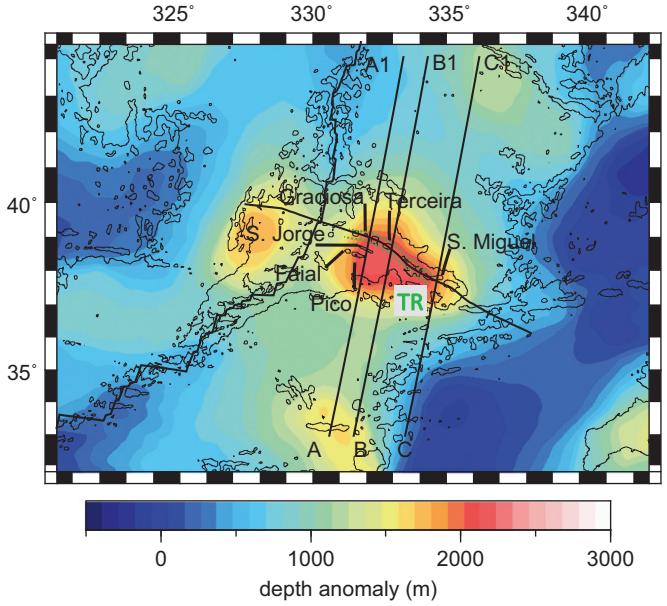

Fig. 5. Depth anomaly obtained by filtering the depth anomaly through the MiFil method (Adam et al., 2005). The black lines are isobaths.

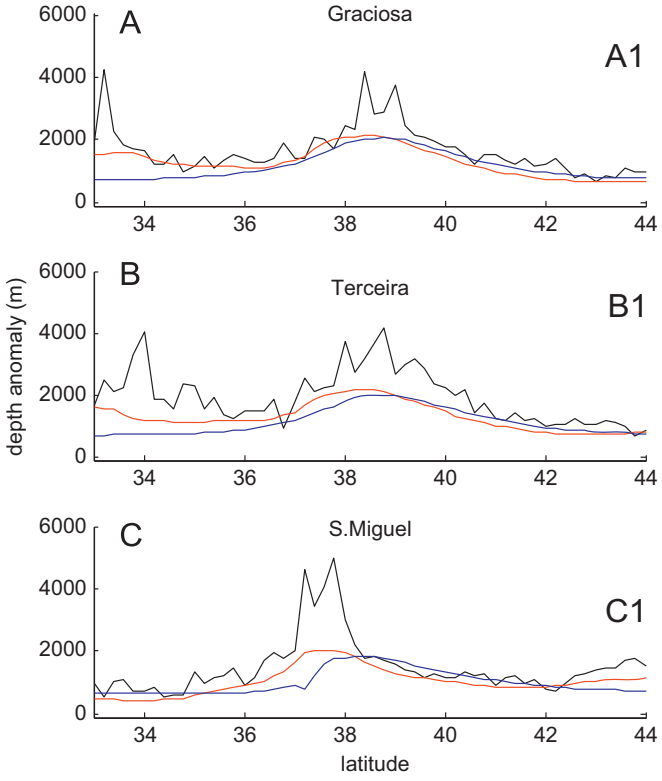

Fig. 6. Depth cross sections of the depth anomaly (black line), the swell, i.e. the filtered depth anomaly (red line) and the dynamic topography (blue line) along the AA1, BB1 and CC1 profiles, which emplacement is represented in Fig. 1.

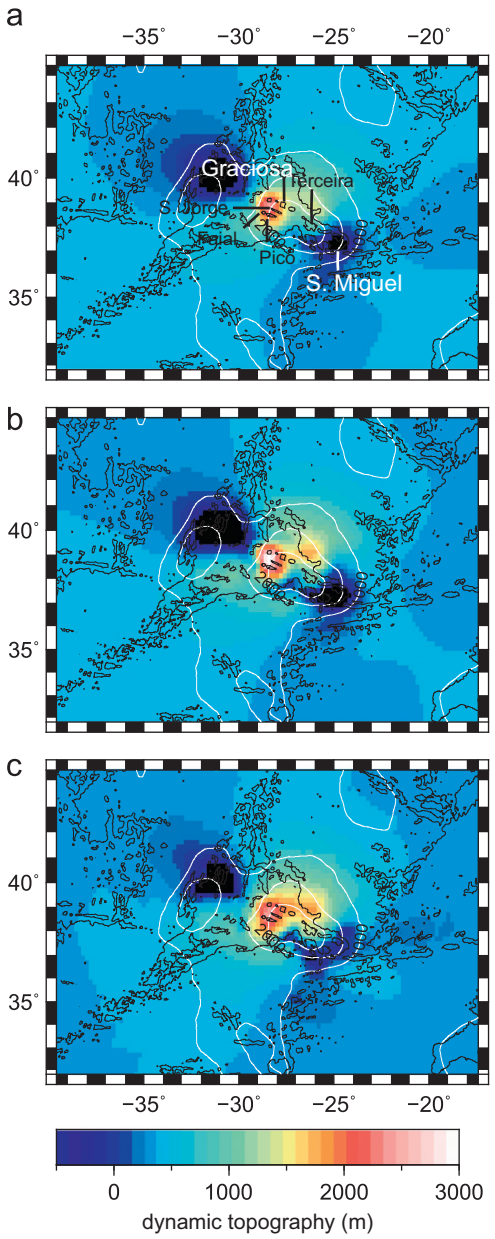

Fig. 7. Dynamic topography obtained by modeling the mantle convection from Yang et al. (2006) tomography model (see text for details). (a) The viscosity is constant. The black lines are isobaths, and the white lines, iscontours of the depth anomaly (Fig. 5). (b) The viscosity is depth and temperature dependent. The depth dependency is imposed by considering a 100 km thick lithosphere. (c) The viscosity is depth and temperature dependent. The depth dependency is imposed by considering the thickening of the lithosphere relatively to the MAR as described by the half-space model.

reflect shallower phenomena. The morphology of the southernmost part of the plateau is characterized by sharp discontinuities, which make us favor Luis et al. (1994) hypothesis, according to which this part of the plateau has been formed by successive NE jumps of the oblique spreading axis.

We also notice a negative depth anomaly west of the mid-Atlantic ridge, between latitudes 40°–41°N, which is due to a downwelling flow created by a cold region situated between the 300- and 500 km depths (Fig. 2). This low is not recovered in the swell. The northernmost part of this region is on the contrary associated with a topographic high (~1500 m). In our model, we have assumed that the seismic velocity anomaly has a thermal origin. However, the velocity anomaly west of the mid-Atlantic ridge may also reflect a different geochemical nature of the mantle. It may correspond to a depleted region, where shallow mantle material has been extracted to feed the mid-Atlantic ridge. In this case, the seismically fast region would be associated with negative density anomalies (Karato, 2008).

However, despite the local departures observed between the dynamic topography and the swell, the mantle dynamics can account for most of the positive depth anomaly associated with the Azores plateau. We therefore conclude that the seafloor elevation is mainly created by the present-day dynamic radial push of the mantle.

3.3. Tractions at the base of the lithosphere

The stresses induced by the mantle convection at the base of the lithosphere ($\tau_{r\theta}$ and $\tau_{r\varphi}$) are displayed in Fig. 8. We have displayed the tractions obtained through the three model previously described, i.e. a model with a constant viscosity (panel a) and two models where the viscosity is depth and temperature dependent (panels b and c). The model in panel b includes a 100 km thick lithosphere, whereas the model displayed in panel c has been computed by imposing the thickening of the lithosphere relatively to the MAR as described by the half-space cooling model.

In Figs. 8 (a and b), the tractions are computed near the surface, whereas in panel c, the tractions are computed at the base of the lithosphere, which thickness varies spatially. When a constant viscosity is imposed (panel a), the traction norm is less than 1 MPa, and the recovered pattern over the TR and the Azores plateau does not allow pertinent interpretation of the dynamics of this region. We do not consider this model realistic. This is also the case for the model displayed in panel b, where the tractions over the TR and the Azores plateau are very weak. On the contrary, the pattern recovered at the base of the lithosphere which thickens relatively to the MAR as described by the half-space model is quite interesting. We have displayed a zoom of this pattern on top of the bathymetry in panel d. Note that whatever the considered viscosity model, a similar pattern is recovered when the tractions ($\tau_{r\theta}$ and $\tau_{r\varphi}$) are computed at the base of the lithosphere. This boundary has a real physical meaning. Under this limit the upper mantle behaves as a viscous fluid. Above this limit, the highly viscous lithosphere behaves as a nearly-rigid body, mechanically coupled with the upper mantle beneath it. In similar studies which investigate the role of mantle convection, the lithosphere is modeled as a high-viscosity layer of fixed thickness. This may not be problematic for intraplate studies, where the base of the lithosphere is very smooth. But in the vicinity of mid-oceanic ridges the thickness of the lithosphere increases very steeply. Ignoring this gradient may lead to the omission of the most important dynamics of the study area. Therefore, considering the tractions occurring at the base of a lithosphere which thickens away from the mid-oceanic ridges is physically justifiable. In the following we will discuss the tractions obtained at the base of the lithosphere which thickens away from the MAR as described by the half space model (panels c and d).

The modeled stresses seem to pull the two edges of the Terceira ridge apart between longitudes 331°E and 334°E, i.e. between the Graciosa Island and the Hirondelle basin. Mantle convection would then be at the origin of the TR opening.

The modeled stresses can also account for the stress field observed through other geophysical observations. Indeed, the seafloor morphology exhibits extension in the western Graciosa Basin, with a N110°E–N120°E trend (Miranda et al., submitted for publication). This trend is recovered by our model. This direction of extension also corresponds to the strike of linear volcanic ridges west of Terceira, and even to the strike of the São Jorge, Pico and

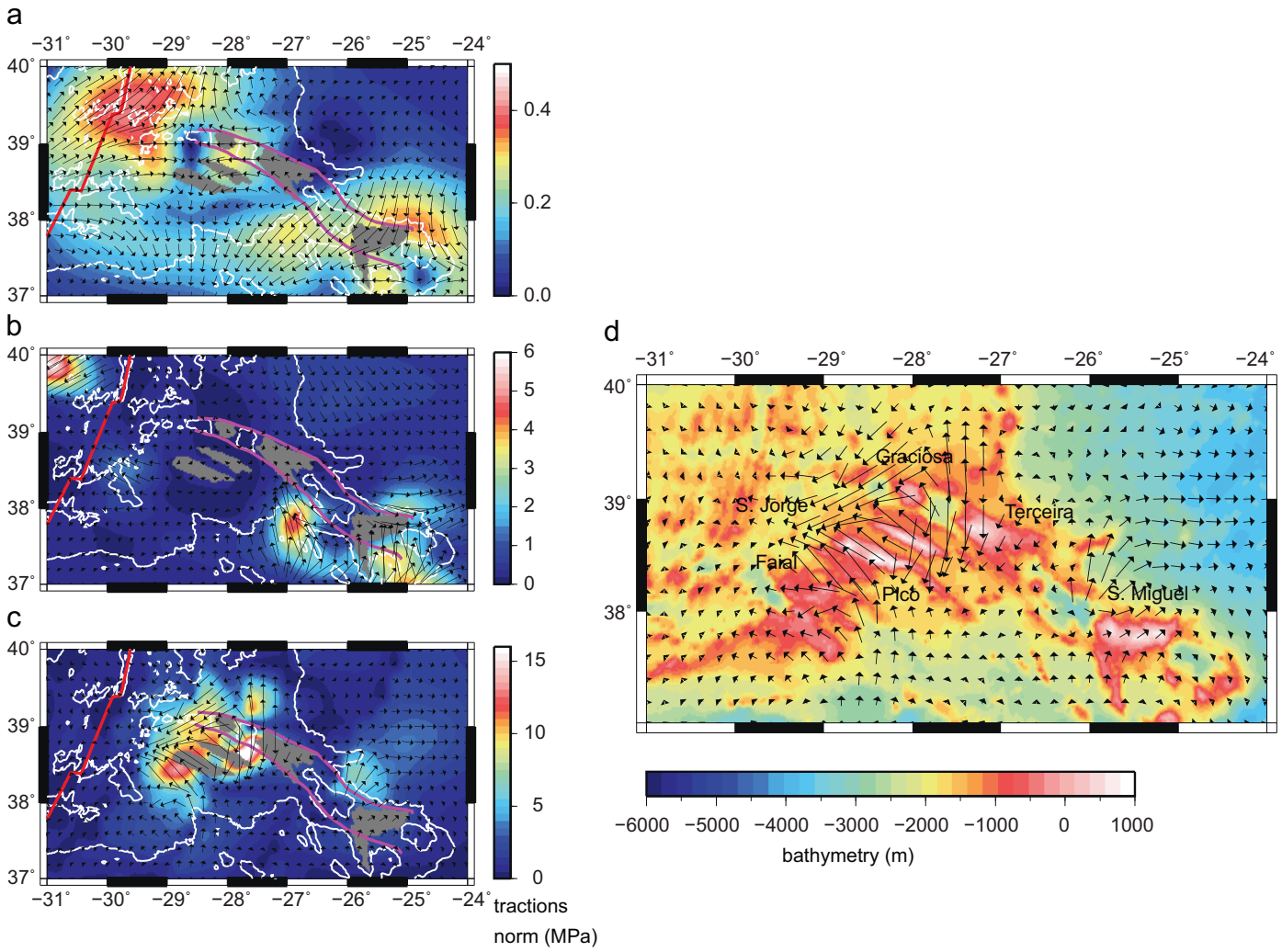

Fig. 8. Tractions induced at the base of the lithosphere by the underlying mantle convection. (a) The viscosity is constant. (b) The viscosity is depth and temperature dependent. The depth dependency is imposed by considering a 100 km thick lithosphere. In the (a) and (b) cases, the tractions are computed at the surface. (c) The viscosity is depth and temperature dependent. The depth dependency is imposed by considering the thickening of the lithosphere relatively to the MAR as described by the half-space model. In this case, the tractions are computed at the base of the lithosphere, which thickness varies spatially. The white line represents the 2000 isobath. The shaded areas represent the 1200 isobath around the S. Miguel, Terceira, Graciosa, S. Jorge, Pico and Faial islands. The MAR and the TR are represented in red and magenta. (d) Zoom on the TR region. The tractions at the base of the lithosphere are the same as in c, and are superimposed on the bathymetry map.

Faial islands, located south of the rift (Lourenço et al., 1998). The study of the geometry of the volcanic cones along the Pico Ridge also shows that the mean direction of the elongation of volcanic cones is 111°N (Stretch et al. 2006). Miranda et al. (submitted for publication) concluded that the observed stress pattern can be due neither to the elastic deformation at the EU–NU plate boundary, nor to ridge push associated with the TR. We show here that the stresses induced by the mantle convection at the base of the lithosphere can account for the observed stress pattern between the Graciosa and S. Miguel islands. West of western Graciosa basin, the stress field is probably affected by the dynamics of the Mid-Atlantic ridge. East of the Hirondelle basin and at S. Miguel Island, our modeled stresses depart from the observations, which may be explained by the prevalence of tectonics induced by plate boundary forces.

The seismic pattern along the Terceira Rift is quite complex. Through the study of *P* and *T* axes obtained from several focal mechanisms, Borges et al. (2007) define two zones of distinct seismicity and stress direction. Zone 1, extending between longitudes 330°E–333°E, corresponded to left-lateral strike–slip faulting with horizontal pressure and tension axes in the E–W and N–S directions. Zone 2, extending between longitudes 333°E to 337°E, corresponded to normal faulting, with a horizontal tension axis trending NE–SW, normal to the Terceira Ridge. Our modeled stresses reproduce well the orientation of the *T*-axis modeled by Borges et al. (2007). The geodynamical model we propose here provides a fair explanation of the seismicity pattern along the Terceira Rift.

3.4. Tectonic regimes and SH directions

The stress tensor computed from our convection model can also be used to predict the tectonic regimes. We use the deviatoric component of the stress tensor to compute the principal stresses τ_1, τ_2, and τ_3 (Heidbach et al. 2008), and the direction of the horizontal shear, SH, (Shmin as well as SHmax) in the latitude/longitude plane.

The results are displayed in Fig. 9. As previously, we have considered several viscosity models, i.e. a model with a constant viscosity (panel a) and two models where the viscosity is depth and temperature dependent (panels b and c). The model in panel b includes a 100 km thick lithosphere, whereas the model displayed in panel c has been computed by imposing the thickening of the lithosphere relatively to the MAR as described by the half-space model.

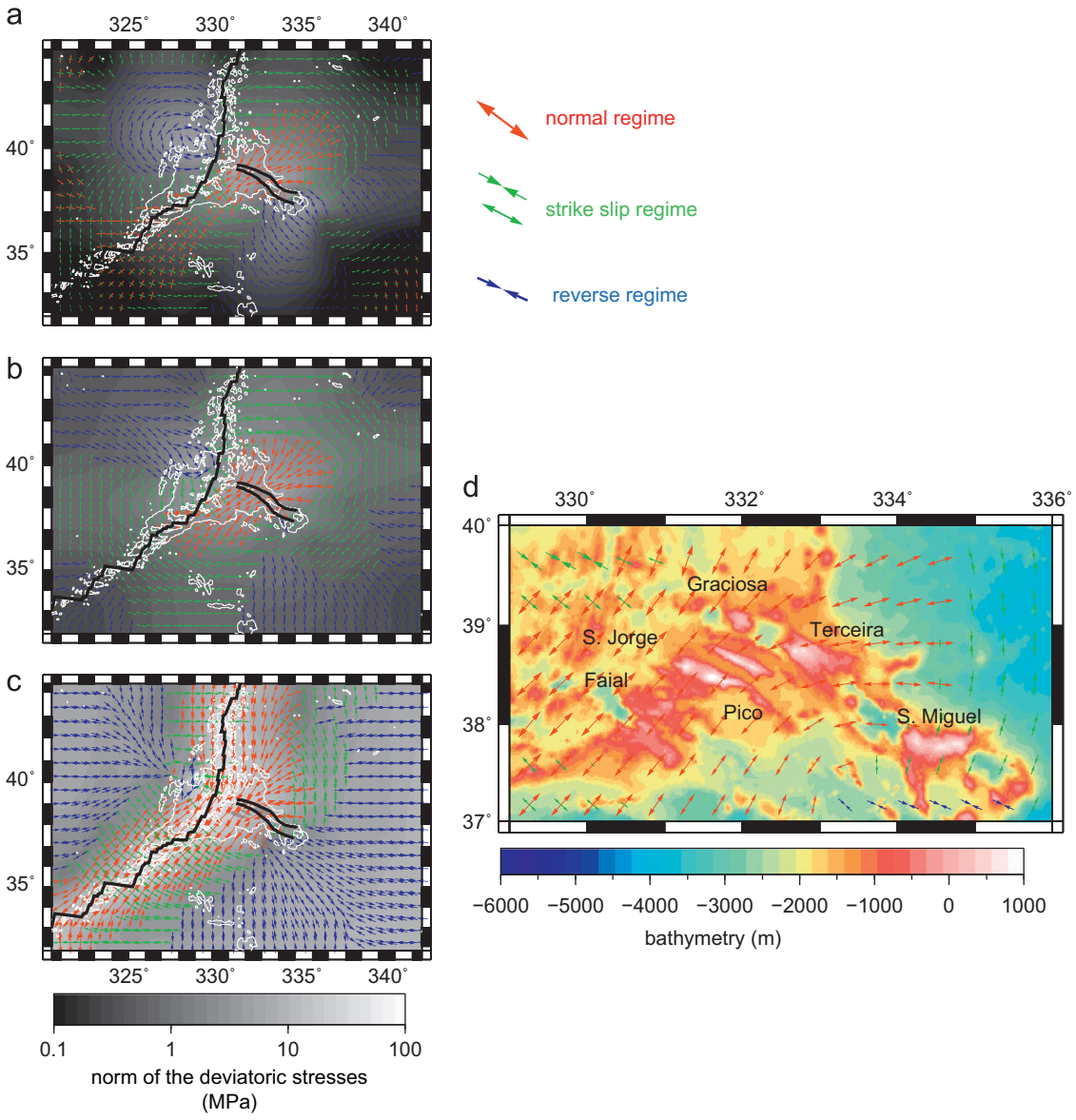

Fig. 9. Tectonic regimes computed from our convection model. The definition of the three tectonics regimes (normal, strikes-slip, thrust fault) is found in Heidbach et al. (2008). The arrows represent the directions of SHmax and Shmin. (a) The viscosity is constant. (b) The viscosity is depth and temperature dependent. The depth dependency is imposed by considering a 100 km thick lithosphere. (c) The viscosity is depth and temperature dependent. The depth dependency is imposed by considering the thickening of the lithosphere relatively to the MAR as described by the half-space model. The white lines are the 2000 isobath. The shaded areas represent the 1200 isobath around the S. Miguel, Terceira, Graciosa, S. Jorge, Pico and Faial islands. The MAR and the contours of the TR are represented in black. (d) Zoom on the TR region. The horizontal stresses are the same as in (c), and are superimposed on the bathymetry map.

For this study, the viscosity model does not influence much the SH pattern over the TR and the Azores plateau, although it influences the regime and SH orientation over the MAR and the NA plate. For all the investigated viscosity models, the TR and the Azores plateau are in an extension regime. The orientation of SHmax varies spatially. The SHmax axes are perpendicular to the directions of S. Jorge, Pico and Faial islands. They are also perpendicular to the western part of the TR, until the Terceira Island. The change of the SHmax directions recovers the *T*-axis directions computed from focal mechanism (Borges et al., 2007). Departures are noticed east of Terceira island, where our modeled SHmax directions are E–W, whereas the *T*-axis are trending NE–SW. However the SH direction is perpendicular to the *P*-axis direction computed by Borges et al. (2007).

In a rifting regime, fracture will develop along directions perpendicular to the direction of SHmax. In our case, the modeled regimes and SH direction can account for the opening of the TR, at least for its western side, and for the morphology of the S. Jorge, Pico and Faial islands. Therefore, we agree with the results of the previous studies stating that the TR is a rifting zone, but we point out to the role of the mantle in the creation of this tectonic regime.

4. Discussion

4.1. Local study

We have conducted a local study to investigate the influence of the mantle dynamics on the geology and tectonics of the Azores region. The Yang et al. (2006) tomography model has been chosen for this purpose since this regional model has enough resolution to resolve the narrow plume structure. However, one can question the pertinence of such a local study. Indeed, such approaches do not take into account the larger scale forces, like the ones driving the plate motions. To investigate the effect of reducing the study area, we have conducted further numerical simulation using the

S40RTS tomography model (Ritsema et al., 2011), a global model which images the shear-velocity structure of the mantle, with a good resolution—up to 40°. We have computed the global mantle flow in the upper mantle, with a numerical resolution of one degree along the horizontal directions, and of 22 km along the radial direction. The number of FVs used is then 32 (in r) × 180 (in θ) × 360 (in φ). The impermeable and shear stress-free conditions are adopted on the top and bottom surface boundaries. The flows across lateral boundaries are taken to be periodic along the longitudinal direction. The S40RTS model has also been used to model the instantaneous flow in a regional study, extending between longitudes 320° and 343°E, and the latitudes 32° and 45°N. The resolution is the same as that for the global study. The number of FVs used is 32 (in r) × 13 (in θ) × 23 (in φ). The flows across lateral boundaries are taken to be symmetric for the local study.

The tectonic regimes and the SH orientations are displayed in Fig. 10. The left panels present the results obtained from the global study, and the local study results are represented in the right side panels. We have displayed the results obtained through the three model previously described, i.e. a model with a constant viscosity (panel a) and two models where the viscosity is depth and temperature dependent (panels b and c). The model in panel b includes a 100 km thick lithosphere, whereas the model displayed in panel c has been computed by imposing the

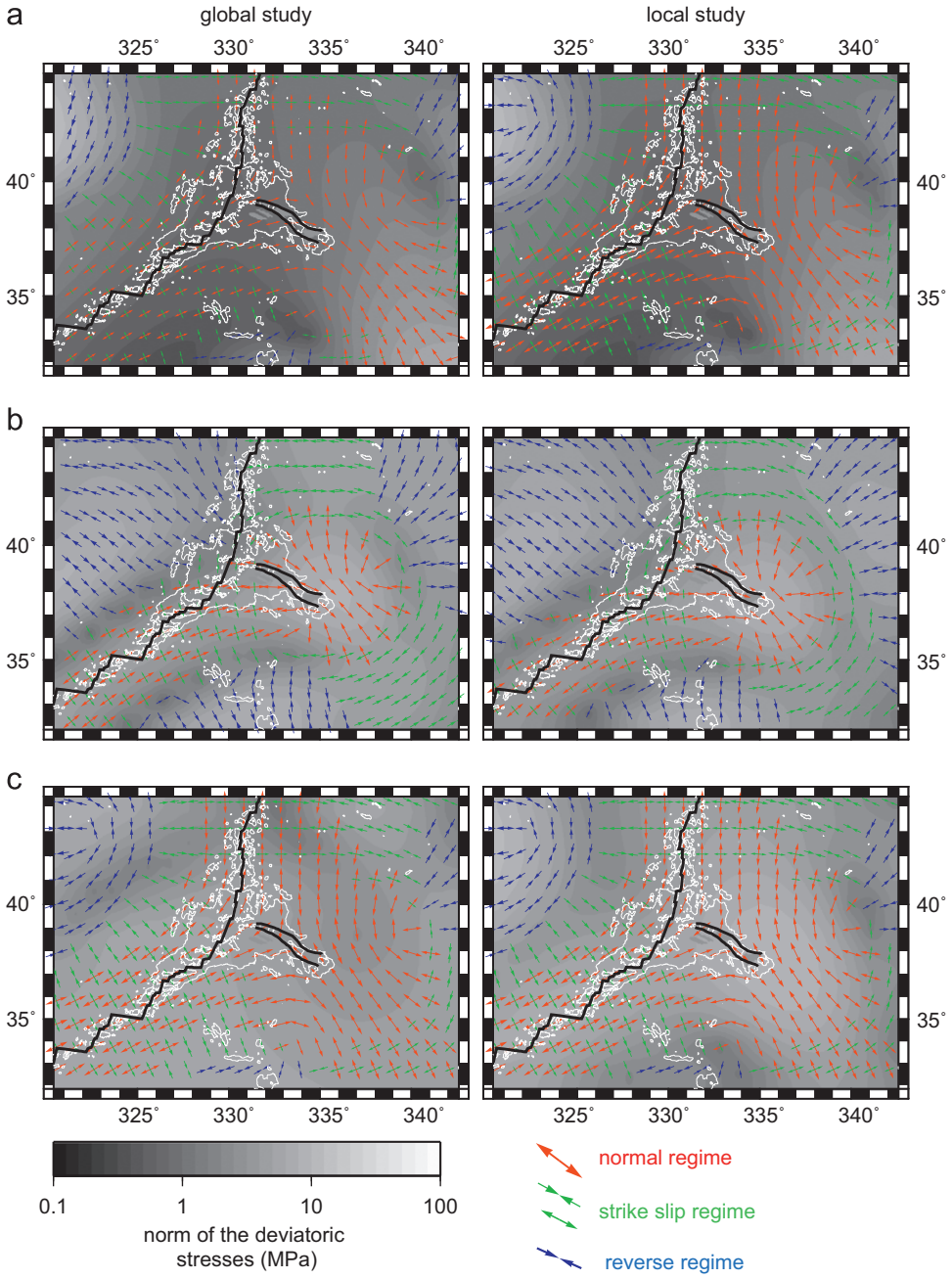

Fig. 10. Tectonic regimes computed from the S40RTS tomography model (Ritsema et al., 2011). The definition of the three tectonics regimes (normal, strikes-slip, thrust fault) is found in Heidbach et al. (2008). The arrows represent the directions of SHmax and Shmin. The left panels present the results obtained from the global study, and the local study results are represented in the right side panels. (a) The viscosity is constant. (b) The viscosity is depth and temperature dependent. The depth dependency is imposed by considering a 100 km thick lithosphere. (c) The viscosity is depth and temperature dependent. The depth dependency is imposed by considering the thickening of the lithosphere relatively to the MAR as described by the half-space model. The white lines are the 2000 isobath. The shaded areas represent the 1200 isobath around the S. Miguel, Terceira, Graciosa, S. Jorge, Pico and Faial islands. The MAR and the contours of the TR are represented in black.

thickening of the lithosphere relatively to the MAR as described by the half-space cooling model.

The horizontal reduction of the study area does not have too important an influence on the modeled stresses. Indeed, the stresses norm and orientation remain roughly the same over the Azores plateau. Changes can be noticed near the boundaries of the study domain, which is neither surprising nor problematic for the present study. Over the Azores plateau, the horizontal reduction of the study area affects mainly the norm of the deviatoric stresses for the viscosity model where the lithospheric thickness increases relatively to the MAR (panel c). This may have important geodynamical inferences, since this norm indicates where the stresses concentration occurs, and therefore where the deformation is more likely to occur. In Fig. 10c, we can see that for the local study the stresses are maximal along the eastern extremity of the Azores plateau and of the TR, although for the global study the stresses seem to concentrate south of the plateau and along the MAR. Actually none of the stress maxima recovered with the S40RTS model seems to precisely account for the geological characteristics of the Azores region. The S40RTS model may lack the accuracy to resolve the narrow structure of the plume and the inferred stresses.

The main conclusion of this section is however that the tectonic regime determination and the computation of the SH orientation does not seem to be too much affected by the reduction of the study area along the horizontal directions. For most of the tested viscosity profiles, the norm of the deviatoric stresses does not change either. Therefore, conducting a local study of the mantle dynamics over the Azores region seems to be justified. This does not mean that such local studies, ignoring the larger scale forces would be correct in any tectonic contexts. But in this precise example, the forces induced by the dynamics of the Azores plume seem to prevail.

4.2. Tomography models

The description of the Azores plume varies according to the different tomography models. We have seen that Yang et al. (2006) model describe a plume associated with negative velocity anomalies in the order of 2%, which displays two main low velocity areas in the shallow mantle, roughly 100–200 km wide. One of the shallow anomalies is centered on the group of islands formed by Faial, Pico, S. Jorge, and Graciosa, the other between the Terceira and S. Miguel islands. These shallow anomalies converge towards one single anomaly, which seems deeply rooted in the upper mantle. Montelli et al. (2006) describe an even deeper root, since their tomography model based on *P* wave inversion reports a plume propagating throughout the whole mantle, and merging with the Canary plume at 1450 km depth. The amplitude of the velocity anomaly associated with the plume in Montelli et al. (2006) model is less than 1%, this means less than half than the one reported by Yang et al. (2006). The radius of the velocity anomaly found by Montelli et al. (2006) is 300 km, i.e. six times wider than the shallow anomalies evidenced by Yang et al. (2006). For Silveira and Stutzmann (2002), the Azores plume is a broad feature, associated with velocities anomalies in the order of 4-5%, propagating at least until the 300 km depth. For these authors, the Azores plume deviates from the ridge axis towards the south in the direction of the Capo Verde hot-spot. Silveira et al. (2006) review the tomographic models under the Azores region and conclude that there is a strong broad negative seismic-velocity anomaly clearly visible at 100 km depth but which disappears below 250–300 km depth.

Considering the great discrepancy of the plume image according to the various tomography models, the choice of the tomography model used as an input will obviously have an important influence on the retrieved mantle convection and the induced stresses. The effects on the dynamic topography are quite obvious: the higher and broader the amplitude of the velocity anomaly, the higher and broader the dynamic topography. This is illustrated in Fig. 11, where we have displayed in the panel (a) the depth cross section of the S40RTS tomography model along the TR. When comparing the Fig. 11(a) with the right side panel in Fig. 2(a), one can see that the plume imaged by the S40RTS model is much broader and is characterized by higher velocity anomalies. The resulting dynamic topography is displayed in Fig. 11(b). It is much wider and has a higher amplitude than the one computed with the Yang et al. (2006) model (Fig. 7). As the plume imaged by the S40RTS model seems to be connected to the MAR, one also recovers some dynamic topography along the MAR. The correlation between the observed depth anomaly (Fig. 5) and the dynamic topography is better when Yang et al. (2006) tomography model is used. Indeed, the location, wavelength and amplitude of the depth anomaly are better recovered by the dynamic topography computed with this model.

The choice of the tomography model used as an input will also have important impact on the stresses calculations. It is difficult to discuss intuitively how the stress pattern will be affected by the tomography model. That is one of the reasons why we have computed the tectonic regimes and the SH orientations from the

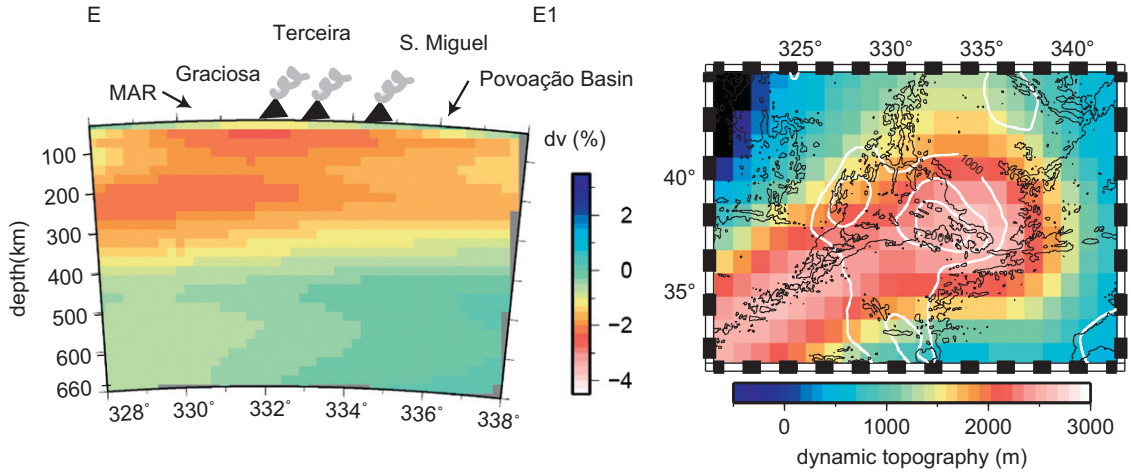

Fig. 11. S40RTS tomography model (Ritsema et al., 2011). (a) depth cross section along the TR–EE1 profile. (b) dynamic topography obtained from the S40RTS tomography model, considering a depth and temperature dependent viscosity law including a highly viscous lithosphere between depths 0 and 100 km.

S40RTS tomography model. They are displayed in Fig. 10, previously discussed. There is an important difference between these results and the ones obtained from Yang et al. (2006) model (Fig. 9). The Azores region is associated with a normal regime, regardless of the tomography model. However, when the S40RTS model is used, the SH direction is no longer perpendicular to the TR and to the islands situated along or south of the TR. In this case, the modeled tectonic regime and stresses cannot account for the TR opening of for the islands emplacement.

When the S40RTS model is used, and when the viscosity law is depth and temperature dependent, with a depth dependency describing a 100 km thick lithosphere (panel b), the modeled stress pattern may be viewed as a classical radial extension field created by the upwelling of a circular plume. There is also an extensional regime along the MAR. The stress field along the MAR does not seem to be so sensitive to the viscosity parameter this time, at the exception of the results displayed in panel b, where we assumed a 100 km thick lithosphere, which may be inappropriate in the vicinity of a mid-oceanic ridge. For the other viscosity laws, the regimes and SH orientations recovered along the MAR are similar to the one found by Ghosh and Holt (2012) and to the stresses extracted from the World Stress Map (Heidbach et al., 2008). The same pattern is also found while using Yang et al. (2006) tomography model and imposing a lithosphere thickening away from the MAR as described by the half-space model (Fig. 9c). Such increase of the lithosphere thickness is actually seen in the S40RTS model.

When the viscosity depth-dependency takes into account the increase of lithosphere thickness away from the MAR, one partially recovers the stress field recovered from Yang et al. (2006) model (Fig. 10c). Indeed, between latitudes 38° and 40°N and longitudes 330° and 333°E the SH direction is perpendicular to the TR and the islands south of the TR. In this case the modeled stresses can account for the opening of the TR or the islands emplacement in this region. This could mean that the viscosity increase perpendicularly to the MAR direction is playing an essential role for determining the tectonic regime in the Azores region. However, when the Yang et al. (2006) model is used instead, such a viscosity law is not required. Moreover the stresses do not seem to be very sensitive to the viscosity law (Fig. 9).

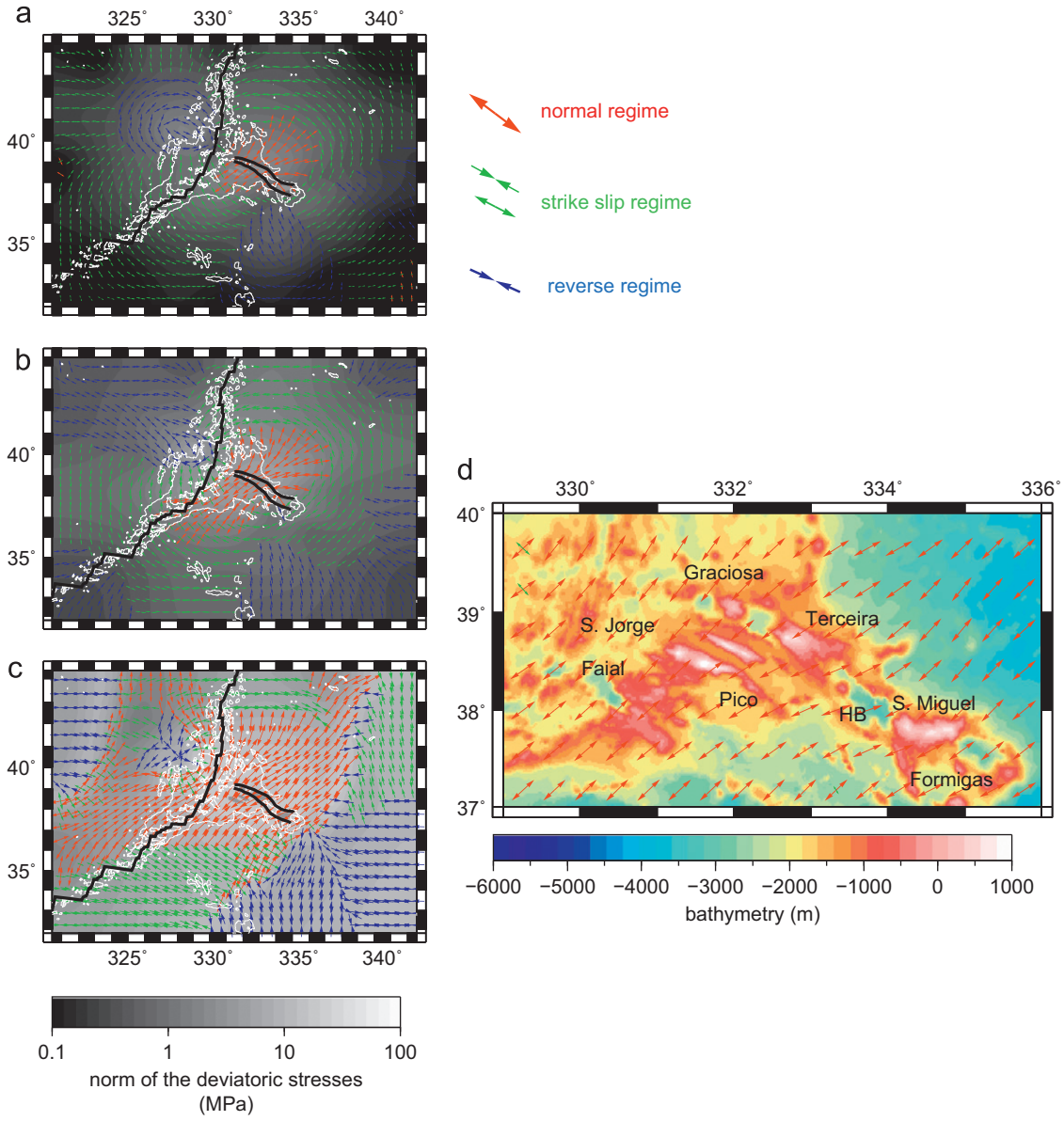

Fig. 12. Same as Fig. 9 except that the density anomaly between depths 0 and 100 km has been replaced by a null density anomaly.

We consider that Yang et al. (2006) tomography model is the most adequate model to investigate the mantle dynamics in the Azores region. Its high resolution allows indeed an accurate resolution of the narrow plume structure. The stresses modeled from this model show a pattern which may account for the complex tectonics of this region. Moreover, the two distinct upwelling imaged by this model can account for the different reservoirs required by the geochemical signatures. However, there are some shortcomings associated with this model. They will be discussed in the next section.

4.3. Accuracy of Yang et al. (2006) model—influence of the shallow mantle

Yang et al.'s tomography model is based on teleseismic body waves. Consequently, the shallow structure (shallower than ~100 km depth) is not well resolved without other constraints. To test the influence of the shallowest part of the mantle, we have made the same calculations exposed earlier in the draft, but we have imposed a zero density anomaly between depths 0 and 100 km, all over the study area. This recovered dynamic topography and tractions at the base of the lithosphere are not very different from the ones we presented earlier, except for a slight decrease in the amplitude of the dynamic topography. We will therefore not present these results here. We will discuss in more details the tectonic regimes and SH orientations. They are displayed in Fig. 12 which can be directly compared with Fig. 9.

There are no major discrepancies between the two sets of results along the Azores plateau. Whatever the chosen viscosity, this region is indeed in an extensional regime, and the SH orientation is perpendicular to the TR and to the Pico, Faial and S. Jorge islands. The modeled stresses can therefore account for the TR opening and the emplacement of these islands. The most important change can be noticed for the test where the lithosphere thickness is increasing away from the MAR (panels c and d in Figs. 9 and 12). When the first 100 km of the tomography were used to model the mantle convection and the induced stresses (Fig. 9c), the normal regime was centered along the MAR. In the test carried out while ignoring the first 100 km (Fig. 12c), the normal regime affects a much more wider region. East of the MAR, the Azores plateau occupies roughly the central position of the region associated with the normal regime. Interestingly, without the first 100 km, one recovers a SH orientation perpendicular to the TR direction along the easternmost part of the TR, between HB and Formigas. Changes in the stress norm and orientation can also be noticed away from the Azores plateau. However, the quality of Yang et al. (2006) tomography model decreases close to the model boundaries. These regions, out of the scope of the present study, should therefore be interpreted carefully.

5. Conclusion

We model the mantle convection in the upper mantle beneath the Azores region. The model is based on the highly resolved tomography model of Yang et al. (2006). Conducting a local study of the mantle dynamics of the Azores region may seem inappropriate since the larger scale forces, like the ones driving the plate motions are omitted. However comparison between local and global mantle flow models, shows that the reduction of the study area along the horizontal directions does not have too significant an effect on the modeled stresses and tectonic regimes. This means that the dynamics induced by the Azores plume is the prevalent force in our study area.

The retrieved convection pattern is complex but points out two distinct upwellings in the shallow mantle. These two reservoirs may account for the different geochemical signatures reported over this area. This also proves that the volcanism emplacement is due to active mantle upwelling. The mantle convection creates a 500 km long, 300 km wide, and 2000 m high positive dynamic topography. It is elongated along the direction of the TR but its maximum is located slightly south of the TR. The dynamic topography recovers well the characteristics of the swell, which implies that most of the depth anomaly associated with the Azores plateau is created by the present-day mantle dynamics. This does not automatically rule out the other physical phenomena, previously invoked to account for the plateau formation. For example rifting is clearly observed in the plateau morphology and may be responsible for the depth anomaly associated with the south-east part of the plateau.

The tractions induced by the mantle convection at the base of the lithosphere are coherent with the rifting direction observed in Terceira Rift basins west of Terceira island (see Miranda et al. (submitted for publication)). We also use the deviatoric component of the stress tensor to compute the stress regime and the SH directions. We find that the Azores plateau and the TR are in a rifting regime. When considering the convection triggered by the density anomalies in the whole upper mantle, our model can account for the seismicity and morphology of the western side of the plateau. Indeed, the direction of SHmax is perpendicular to the S. Jorge, Pico and Faial islands, and to the extensional features with similar trend. However, the shallow structure of the mantle is not well resolved by the tomography models based on teleseismic body waves. While ignoring this shallowest part of the Yang et al. (2006) tomography model, one also recovers the seismicity and morphology characteristics of the eastern side of the plateau. The role of mantle convection in triggering the rifting regime and the northward jumps of the Azores triple junction has already been invoked by former studies. Here we quantitatively assess this mantle contribution.

Acknowledgements

This work is supported by the Fundaçãopara a Ciência e a Tecnologia (OREAZ project PTDC/CTE-GIX/102061/2008). We would like to thank T. Yang for providing us his tomography model and two anonymous reviewers for their useful suggestions which improved the manuscript.

References

Adam, C., Vidal, V., Bonneville, A., 2005. MiFil: a method to characterize hotspot swells with application to the South Central Pacific. Geochem. Geophys. Geosyst. 6, Q01003, http://dx.doi.org/10.1029/2004GC000814.

Adam, C., Bonneville, A., 2005. Extent of the South Pacific superswell. J. Geophys. Res. 110, B09408, http://dx.doi.org/10.1029/2004JB00346.

Adam, C., Yoshida, M., Isse, T., Suetsugu, D., Fukao, Y., Barruol, G., 2010. South Pacific hotspot swells dynamically supported by mantle flows. Geophys. Res. Lett. 37, L08302, http://dx.doi.org/10.1029/2010GL042534.

Beier, C., Stracke, A., Haase, K.M., 2007. The peculiar geochemical signatures of São Miguel lavas: metasomatised or recycled mantle sources? Earth Planet. Sci. Lett. 259 (1–2), 186–199, http://dx.doi.org/10.1016/j.epsl.2007.04.038.

Borges, J.F., Bezzeghoud, M., Buforn, E., Pro, C., Fitas, A., 2007. The 1980, 1997 and 1998 Azores earthquakes and some seismo-tectonic implications. Tectonophysics 435, 37–54.

Bougault, H., Treuil, M., 1980. Mid-Atlantic Ridge: zero-age geochemical variations between Azores and 22°N. Nature 286, 209–212.

Bougault, H., Cande, S.C., 1985. Background, objectives and summary of principal results: deep sea drilling project sites 556–564. Deep Sea Drill. Proj. Initial Rep. 82, 5–16.

Cannat, M., Briais, A., Deplus, C., Escartin, J., Georgen, J., Lin, J., Mercouriev, S., Meyzen, C., Muller, M., Pouliquen, G., Rabain, A., Silva, P., 1999. Mid-Atlantic Ridge-Azores hotspot interactions: along-axis migration of a hotspot-derived event of enhanced magmatism 10 to 40 Ma ago. Earth Planet. Sci. Lett. 173, 257–269.

Cole, P.D., Guest, J.E., Duncan, A.M., Pacheco, J.-M., 1995. An historic subplinian/phreatomagmatic eruption: the 1630 A.D. eruption of Furnas volcano, SãoMiguel, Azores. J. Volcanol. Geotherm. Res. 69, 117–135.

Cole, P.D., Guest, J.E., Duncan, A.M., Pacheco, J.-M., 2001. Capelinhos 1957–1958, Faial, Azores: deposits formed by an emergent surtseyan eruption. Bull. Volcanol. 63, 204–220.

Davies, G.R., Norry, M.J., Gerlach, D.C., Cliff, R.A., 1989. A combined chemical and Pb–Sr–Nd isotope study of the Azores and Cape Verde hot-spots: the geodynamic implications. In: Saunders, A.D., Norry, M.J. (Eds.), Magmatism in the ocean basins. Geol. Soc. Special Publication, 42; 1989, pp. 231–235.

Dosso, L., Bougault, H., Langmuir, C., Bollinger, C., Bonnier, O., Etoubleau, J., 1999. The age and distribution of mantle heterogeneity along the Mid-Atlantic Ridge (31–41 degrees N). Earth Planet. Sci. Lett. 170, 269–286.

Dziewonski, A.M., Anderson, D.L., 1981. Preliminary reference Earth model. Phys. Earth Planet. Inter. 25, 297–356.

Elliott, T., Blichert-Toft, J., Heumann, A., Koetsier, G., Forjaz, V., 2007. The origin of enriched mantle beneath São Miguel, Azores. Geochim. Cosmochim. Acta 71 (1), 219–240, http://dx.doi.org/10.1016/j.gca.2006.07.043.

Escartín, J., Cannat, M., Pouliquen, G., Rabain, A., Lin, J., 2001. Crustal thickness of V-shaped ridges south of the Azores: interaction of the Mid-Atlantic Ridge (36°-39°N) and the Azores hot spot. J. Geophys. Res 106, 21719–21735.

Gaspar, J.L., Queiroz, G., Pacheco, J.M., Ferreira, T., Wallenstein, N., Almeida, M.H., Coutinho, R., 2003. Basaltic lava balloons producing during the 1998–2001 Serreta Submarine Ridge eruption (Azores). Geophys. Monogr. 140, 205–212.

Gente, P., Dyment, J., Maia, M., Goslin, J., 2003. Interactions between the MAR and the Azores hot spot during the last 85 Myr: emplacement and rifting of the hot spot-derived plateaus. Geochem. Geophys. Geosyst. 4, 1–23.

Georgen, J.E., Sankar, R.D., 2010. Effects of ridge geometry on mantle dynamics in an oceanic triple junction region: implications for the Azores Plateau. Earth Planet. Sci. Lett. 298, 23–34.

Ghosh, A., Holt, W.E., 2012. Plate Motions and Stresses from Global Dynamic Models. Science 335, 838.

Heidbach, O., Tingay, M., Barth, A., Reinecker, J., Kurfeß, D., Müller, B., 2008. The World Stress Map Database Release . http://dx.doi.org/10.1594/GFZ.WSM.Rel2008.

Karato, S.I., 2008. Deformation of Earth Materials: an Introduction to the Rheology of Solid Earth. Cambridge University Press, New York.

Kennett, B.L.N., Engdahl, E.R., 1991. Travel times for global earthquake location and phase association. Geophys. J. Int. 105, 429–465.

Krause, D.G., Watkins, R.B., 1970. North Atlantic crustal genesis in the vicinity of the Azores. Geophys. J. R. Astron. Soc. 19, 261–263.

Lourenço, N., Miranda, J.M., Luis, J.F., Ribeiro, A., Mendes-Victor, L.A., Madeira, J., Needham, H.D., 1998. Morpho-tectonic analysis of the Azores Volcanic Plateau from a new bathymetric compilation of the area. Mar. Geophys. Res. 20, 141–156.

Luis, J.F., Miranda, J.M., Patriat, P., Galdeano, A., Rossignol, J.C., Mendes-Victor, L., 1994. Açores Triple Junction Evolution in the last 10 ma from a New Aeromagnetic Survey,. Earth Planet. Sci. Lett. 125, 439–459.

Luis, J.F., Neves, M.C., 2006. The isostatic compensation of the Azores Plateau: a 3D admittance and coherence analysis. J. Volcanol. Geotherm. Res. 156 (2006), 10–22.

Luis, J.F., Miranda, J.M., 2008. Re-evaluation of Magnetic Chrons in the North-Atlantic between 35°N and 47°N: implications for the formation of the Azores triple junction and associated plateau. J. Geophys. Res. 113, B10.

Luis, J.M., Miranda, J.M., Lourenco, N., Moulin, M., 2009. Improved magnetic compilation for the Central North Atlantic based on new data from the Portuguese UNCLOS proposal and CM4 model. American Geophysical Union, Fall Meeting 2009, abstract GP13C-0778.

Machado, F., 1959. Actividade vulclnica da ilha do Faial. Atlântida, orgão do Inst. Açoriano de Cultura. vol. Ill, no. 1, e 3, Angra do Heroísmo.

Madeira, J., Ribeiro, A, 1990. Geodynamic models for the Azores triple junction: a contribution from tectonics. Tectonophysics 184, 405–415.

Madureira, P., Moreira, M., Mata, J., Allègre, C.J., 2005. Primitive helium and neon isotopes in Terceira Island: constraints on the origin of the Azores archipelago. Earth Planet. Sci. Lett. 233, 429–440.

Madureira, P.J., Mata, Mattielli, N., Queiroz, G., Silva, P., 2011. Mantle source heterogeneity, magma generation and magmatic evolution at Terceira Island (Azores archipelago): Constraints from elemental and isotopic (Sr, Nd, Hf, and Pb) data. Lithos 126, 402–418.

Maia, M., C. Hémond, Gente P., 2001. Contrasted interactions between plume, upper mantle, and lithosphere: foundation chain case. Geochem. Geophys. Geosyst., 2, paper number 2000GC000117.

McKenzie, D.P., 1972. Active tectonics of the Mediterranean region. Geophys. J. R. Astron. Soc. 30, 109–185.

Miranda, J.M., Luis, J.F., Lourenco, N. Azores Triple Junction: no discrete boundary close to the Mid-Atlantic Ridge. Geology, submitted for publication.

Montelli, R., Nolet, G., Dahlen, F.A., Masters, G., Engdahl, R.E., Hung, S.H., 2004. Finite-frequency tomography reveals a variety of plumes in the mantle. Science 303, 338–343.

Montelli, R., Nolet, G., Dahlen, F.A., Masters, G., 2006. A catalogue of deep mantle plumes: new results from finite frequency tomography. Geochem. Geophys. Geosyst. 7, Q11007, http://dx.doi.org/10.1029/2006GC001248.

Moore, R.B., 1990. Volcanic geology and eruption frequency, São Miguel, Azores. Bull. Volcanol. 52, 602–614.

Moreira, M., Doucelance, R., Dupré, B., Kurz, M., Allègre, C.J., 1999. Helium and lead isotope geochemistry in the Azores archipelago. Earth Planet. Sci. Lett. 169, 189–205.

Morgan, W., 1971. Convection plumes in the lower mantle. Nature 230, 42–43.

Ritsema, J., Deuss, A., van Heijst, H.J., Woodhouse, J.H., 2011. S40RTS: a degree-40 shear-velocity model for the mantle from new Rayleigh wave dispersion, teleseismic traveltime and normal-mode splitting function measurements. Geophys. J. Int. 184 (3), 1223–1236.

Schilling, J.-G., 1985. Upper mantle heterogeneities and dynamics. Nature 314, 62–67.

Self, S., 1976. The recent volcanology of Terceira, Azores. J. Geol. Soc. London 132, 645–666.

Silveira, G., Stutzmann, E., 2002. Anisotropic tomography of the Atlantic Ocean. Phys. Earth Planet. Inter. 132, 237–248.

Silveira, G., Stutzmann, E., Davaille, A., Montagner, J.-P., Mendes-Victor, L., Sebai, A., 2006. Azores hotspot signature in the upper mantle. J. Volcanol. Geotherm. Res. 156, 23–34.

Stretch, R.C., Mitchell, N.C., Portaro, R.A., 2006. A morphometric analysis of the submarine volcanic ridge south-east of Pico Island, Azores. Journal of Volcanology and Geothermal Research 156, 35–54.

Stein, C.A., Stein, S., 1992. A model for the global variation in oceanic depth and heat-flow with lithospheric age. Nature 359, 123–129.

Turcotte, D.L., Schubert, G., 2001. Geodynamics, second ed. Cambridge University Press, New York, 456 pp.

Turner, S., Hawkesworth, C., Rogers, N., King, P., 1997. U–Th isotope disequilibria and ocean islands basalt generation in the Azores. Chem. Geol. 139, 145–164.

Vogt, P.R., Jung, W.Y., 2004. The Terceira Rift as hyper-slow, hotspot-dominated oblique spreading axis: a comparison with other slow-spreading plate boundaries. Earth Planet. Sci. Lett. 218, 77–90.

White, W.M., Tapia, M.D.M., Schilling, J.-G., 1979. The petrology and geochemistry of the Azores Islands. Contrib. Mineral. Petrol. 69, 201–213.

Yang, T., Shen, Y., van der Lee, S., Solomon, S.C., Hung, S.H., 2006. Upper mantle structure beneath the Azores hotspot from finite-frequency seismic tomography. Earth Planet. Sci. Lett. 250, 11–26.

Yoshida, M., 2008. Core–mantle boundary topography estimated from numerical simulations of instantaneous mantle flow. Geochem. Geophys. Geosyst. 9, Q07002, http://dx.doi.org/10.1029/2008GC002008.